

Three Spectacular HII-buried-AGN Galaxies from SDSS

Yufeng Mao^{1,2}, Jing Wang¹, & Jianyan Wei¹

ABSTRACT

We present our analysis of the three HII-buried-AGN: SDSS J091053+333008, SDSS J121837+091324, and SDSS J153002-020415, by studying their optical spectra extracted from SDSS. The location in the BPT diagnostic diagrams of the three galaxies indicates that the narrow emission lines are mainly excited from HII regions. However, after the removal of the host galaxy’s stellar emission, the emission lines display the typical feature of Narrow-line Seyfert 1-like. All of the three objects have large Eddington ratio, small black hole mass, and low star formation rate. We propose that the three galaxies are at the transit stage from the starburst-dominated phase to AGN-dominated phase.

Subject headings: galaxies: active — quasars: emission lines — quasars

1. Introduction

In recent years, there have been remarkable evidences that the evolution of supermassive black hole (SMBH) and its host galaxy are tightly linked. The significant correlation between the mass of the SMBH and the velocity dispersion of the bulge where the SMBH resides in implies that there exists a tight relation between AGN activity and star formation in the bulge (e.g. Magorrian et al. 1998; Shields et al. 2003; Greene & Ho 2006; Tremaine et al. 2002; Ferrarese et al. 2006). It is now clear that AGN activity and star formation frequently happen together (e.g. Gonzalez Delgado 2002). A specific example is the “Q+A” galaxies, characterized by composite spectra displaying broad emission lines as well as Balmer absorption lines of A-type stars (e.g., Brotherton et al. 1999; Zhou et al. 2005; Wang & Wei, 2006; Goto 2006; Wild et al. 2007).

¹National Astronomical Observatories, Chinese Academy of Sciences, Beijing 100012, China; myf@bao.ac.cn

²Graduate University of Chinese Academy of Sciences, Beijing, P.R.China

Accumulating studies show a likely evolution sequence of co-evolution of AGN and star formation. Using the large SDSS spectra database, Heckman et al. (2004) found that most accretion occurs onto the black holes with high stellar surface mass densities and young stellar populations. Wang et al. (2006) found that the well-documented Eigenvector 1 (E1) space (Boroson & Green, 1992; hereafter BG92) could be extended to the infrared color $\alpha(60,25)$. They argued that AGNs might evolve along with the E1 space. Wang & Wei (2008) recently studied a sample of partially obscured AGNs from SDSS. The broad $H\alpha$ emission inferred Eddington ratio (L/L_{Edd}) is found to decrease with age of stellar population. This result is consistent with the studies of Kewley et al. (2006) and Wild et al. (2007), who estimated L/L_{Edd} indirectly through $L([\text{OIII}])/\sigma_*$ for obscured AGNs.

However, we still know very little about the details of the co-evolution of the starbursts and SMBH. For instance, do AGN activity trigger starbursts (e.g. Goncalves et al. 1999), or starbursts trigger AGN activity (e.g. Weedman 1983), or they happen at the same time and co-evolve together? There are some suggestions from the works on the highest redshift quasar that the black holes form prior to the assembly of the stellar bulges (Walter et al. 2004; Riechers et al. 2008). Numerical simulations of galaxies merger including SMBHs developed a theoretical light curve of central AGN activity (Di Matteo et al. 2005; Springel et al. 2005). In this model, for most of the duration of the starburst, the black hole is “buried”, being heavily obscured by surrounding gas and dust, especially in UV/optical bands (Hopkins et al. 2005a,b). If so, we would expect to identify some AGNs with their narrow emission lines dominantly exited from H II region, indicating that the central AGNs are surrounded by the gas or dust of the H II region.

In this paper, we report the identification of three “HII-buried-AGN” from SDSS Data Release 4 (DR4, Adelman-McCarthy et al. 2006) MPA/JHU catalog¹. They are SDSS J091053+333008, SDSS J121837+091324, and SDSS J153002-020415. Their redshifts are 0.116 ± 0.001 , 0.078 ± 0.001 , and 0.051 ± 0.001 , respectively. All of the three objects show typical AGN features, such as power-law continuum, broad emission line of $H\alpha$ and $H\beta$, and even strong optical Fe II emissions. However, by fitting the narrow emission lines, we can determine that all of the three objects are located in the H II regions in the BPT diagnostic diagrams (Baldwin et al. 1981). The paper is structured as follows. We present the objects selection in §2, and introduce the spectral analysis in §3. The results and discussions are presented in Section 4 and 5, respectively. The Λ cold dark matter (Λ CDM) cosmology with $\Omega_m = 0.3$, $\Omega_\Lambda = 0.7$, and $H_0 = 70 \text{ km s}^{-1} \text{ Mpc}^{-1}$ (Spergel et al. 2003) is assumed throughout this paper.

¹The catalogs could be downloaded from <http://www/mpa-garching.mpg.de/SDSS/>.

2. Objects selection

Because the blueshifted [OIII] emission is thought to be an indicator of outflows in AGN (e.g. Boroson 2005; Komossa et al. 2008), our primary motivation is to compare the different properties of blueshifted [OIII] profile between star-forming galaxies and Seyferts + LINERs, and results will be presented in subsequent papers. We start our objects selection from SDSS DR4 MPA/JHU catalogues (Kauffmann et al. 2003; Heckman et al. 2004). The catalogs contain a set of physical properties of 567,486 emission-line galaxies, including Seyferts, LINERs, and star-forming galaxies. To ensure our sample have a high quality in spectra, we need our sample have a median S/N larger than 20 across the whole spectrum. Especially, we need the [OIII] and $H\beta$ emission lines have S/N larger than 40. About 3200 star-forming galaxies have been selected according to the criteria. Then we focus on the 200 star-forming galaxies which show the largest [OIII] blueshift ($\sim 100 \text{ km s}^{-1}$), and check their spectra by eyes carefully. Only three objects among them, SDSS J091053+333008, SDSS J121837+091324, and SDSS J153002-020415, display typical AGN features, such as broad Balmer emission lines and FeII complex, superposed on spectra of young stellar population stars. The evident AGN features motivate us to carefully re-examine the spectra properties for these three objects.

3. Spectral analysis

The spectral reduction is performed by standard IRAF procedures. By assuming the Galactic extinction curve with $R_V = 3.1$, each spectrum is corrected for Galactic extinction correction following the reddening maps of Schlegel et al. (1998). Each of the extinction-corrected spectrum is transformed to the rest frame, along with k -correction, according to the corresponding redshift provided by the SDSS pipelines. The spectra at the rest frame are displayed in Figure 1.

For SDSS J091053+333008, because its star light is so weak that the spectrum is dominated by AGN’s featureless continuum and broad emission lines, we fit the continuum by the combination of a free powerlaw and the Fe II template provided by BG92. The FWHM of the FeII template is fixed to that of its $H\beta$ broad component (e.g., BG92; Hu et al. 2008). For the other two objects, the star light components are removed by the principal component analysis (PCA) technique (e.g. Li et al. 2005; Hao et al. 2005; Wang & Wei 2008). Briefly, a library of pure stellar absorption-line spectra (eigen-spectra) is built by applying the PCA method on the single stellar population (SSP) models developed by Bruzual & Charlot (2003, hereafter BC03). The range of ages for these models is between 1×10^5 and 2×10^{10} yr. In our fitting progress, several components are adopted and listed as follows: the first seven eigen-

spectra, an FeII complex template from BG92, and a Galactic extinction curve (Cardelli et al. 1989). A χ^2 minimizing algorithm is performed to determine the stellar absorption spectrum for each galaxy over the wavelength range from 3700-6800 Å, except for the regions around the strong emission lines: H α , H β , [NII] $\lambda\lambda$ 6548, 6584, [OIII] $\lambda\lambda$ 4959, 5007, and [OII] λ 3727. The left column of Figure 1 shows the results of the AGN continuum/starlight removal, the modeled FeII complex, and the isolated AGN emission-line spectra.

The AGN emission-line spectra are then modeled by the multi-components modeling procedure (SPECFIT task in IRAF package) as introduced by Kriss (1994). Each emission line is modeled by a set of Gaussian profiles. We model each of the H α , H β and [OIII] emission line profiles by two Gaussians: one broad and one narrow components. The width of [OIII] λ 5007_n is set to be the same as that of H β _n. Both intensity ratios [O III] λ 5007/ λ 4959 and [N II] λ 6583/ λ 6548 are fixed to be 3.0. The profile modelings for the H α and H β regions are illustrated in Figure 1 (middle and right columns). The results of the line profile modelings are shown in Table 1. All the uncertainties given in Table 1 are caused by the profile modelings.

4. RESULTS

4.1. Star-forming origin for narrow emission lines

Basing upon a set of line ratios, such as [OIII]/H β , [NII]/H α , [SII]/H α , and [OI]/H α , the BPT diagrams are commonly used as a powerful tool to determine the dominant energy source in the emission-line galaxies. Comparing with star-forming galaxies, AGNs (Seyferts and LINERs) have larger line ratios because of their stronger and harder ionizing field. The theoretical demarcation lines determine the lower limit of AGNs (Seyfert and LINERs) were proposed by Kewley et al. (2001) according to their theoretical stellar photoionization models. Using the large spectra database provided by SDSS, Kauffmann et al. (2003) proposed an empirical demarcation line separating star-forming galaxies in the [OIII]/H β vs. [NII]/H α diagram.

Because the Balmer line profiles are modeled by a combination of a broad and a narrow components in the three objects, it is therefore necessary to re-examine their locations on the BPT diagrams in the current study. The three objects are plotted in the BPT diagrams in Figure 2. The four panels represent the four different pairs of line ratios. It is clear that all the three objects are below the theoretical demarcation lines (see Panel A, B and C) proposed in Kewley et al. (2001). In particular, SDSS J091053+333008 is obviously located in the HII region in the [O III]/H β vs. [N II]/H α diagram, i.e, far below the empirical

classification line suggested by Kauffmann et al. (2003). In the same diagram, the other two objects are located marginally above the empirical demarcation line. Since the objects are extracted from star-forming galaxies from the MPA/JHU catalog, the reason why they are not located in the HII region is that we have removed the broad component of $H\alpha$ and $H\beta$. As a result, the ratio of $[OIII]/H\beta$ and $[NII]/H\alpha$ might be a little different from Kauffmann et al. (2003).

As an additional test, we plot the three objects on the $[O III]/[O II]$ vs. $[O I]/H\alpha$ diagram in Panel D in Figure 2. The line ratio of $[O III]/[O II]$ is sensitive to the ionization parameter of the gas (Kewley et al. 2006). To obtain the line ratio, we need to correct the intrinsic dust extinction on the flux of $[O III]$ and $[O II]$. For each object, the extinction is estimated from the observed Balmer decrement for narrow components of $H\alpha$ and $H\beta$, assuming the Case B recombination. The predicted $H\alpha/H\beta$ ratio is 2.86 for H II region in the condition of gas density 100cm^{-3} and temperature 10^4K (Osterbrock 1989). The derived A_v values $[=R_v \times E(B-V)]$ are listed in Table 1 for the three objects. As shown in the diagram, all of our three objects are located in the region occupied by star-forming galaxies.

In summary, using the widely used diagnostic tools, we draw a conclusion that the narrow emission lines in the three objects are mainly powered by the ionizing field from hot stars rather than AGNs.

After demonstrating that the narrow emission lines are mainly powered by star formation activity, we attempt to estimate current star formation rate for the three objects in terms of the $[O II]\lambda 3727$ emission. $[O II]\lambda 3727$ is an empirical indicator to estimate the current star formation rate (SFR) for emission-line galaxies (e.g. Gallagher et al. 1989; Kennicutt 1998; Kewley et al. 2004). We calculate the SFR according to the equations in Kewley et al. (2004):

$$\text{SFR}([OII]) = \frac{7.9 \times 10^{-42} L([OII]) (\text{ergss}^{-1})}{(-1.75)[\log(O/H) + 12] + 16.73} M_{\odot} \text{yr}^{-1} \quad (1)$$

The metallicity is estimated according to the empirical calibration using the R_{23} indicator (Kewley et al. 2004), where $R_{23} = \log([OII]\lambda 3727 + [OIII]\lambda 5007)/H\beta$. Again the $[O II]$ luminosity is corrected for the intrinsic extinction derived from the Balmer decrement. The calculated current SFRs of the three objects are listed in Table 1. It turns out that all of them have small $\text{SFR} \sim 1 M_{\odot} \text{yr}^{-1}$, which indicates a suppressed star formation activity likely due to the AGN feed back (see below for discussion of AGN properties).

4.2. Broad emission lines: an indicative of AGNs

The AGN properties are examined in this section. The detection of broad Balmer emission lines is an indicative of the existence of AGN in the center of galaxy (see Section 4 for the discussion of other origins). Our spectral measurements indicate that all of the three objects show AGN line emission with relatively narrow $H\beta$ profiles and large Fe II ratios, which are the typical features of Narrow-line Seyfert 1 Galaxies (NLS1s, e.g., Osterbrock & Pogge 1985). The measured FWHMs of $H\beta$ broad emission lines are around 2000 km s^{-1} , and the Fe II ratios $R_{\text{Fe}} \sim 2$ (except SDSS 153002-020415), where the R_{Fe} is defined as the flux ratio of optical Fe II/ $H\beta_{\text{B}}$. The flux of the Fe II blends is measured between the rest frame wavelength 4434 and 4684 \AA . Especially, the object SDSS J121837+091324 has already been included in the ~ 2000 NLS1 galaxies sample from SDSS by Zhou et al. (2006).

The co-evolution of AGN and its host galaxy implies that young AGNs are associated with young stellar population and intensive star formation activity. Mathur (2000) proposed that NLS1s with small black hole mass (M_{BH}) and high Eddington ratio (L/L_{Edd}) are at early stage of evolution of AGN. The evident broad emission lines allow us to study the black hole accretion directly in the three objects. The black hole mass (M_{BH}) and Eddington ratio (L/L_{Edd}) are two basic physical parameters of AGNs (e.g. BG92; Boroson 2002). We refer the readers to McGill et al. (2008) for a summary of the existing formula used to estimate M_{BH} basing upon “single-epoch” spectrum. These methods are based on the great progress in the calibration of the $R_{\text{BLR}} - L$ relationship (e.g., Kaspi et al. 2007 and references therein). In the current study, we estimate the M_{BH} for the three objects according to their broad $H\alpha$ and $H\beta$ emission lines (Greene & Ho 2005):

$$M_{\text{BH}} = 2 \times 10^6 \left(\frac{L_{\text{H}\alpha}}{10^{42} \text{ ergs s}^{-1}} \right)^{0.55} \left(\frac{\text{FWHM}(\text{H}\alpha)}{1000 \text{ km s}^{-1}} \right)^{2.06} M_{\odot} \quad (2)$$

$$M_{\text{BH}} = 3.6 \times 10^6 \left(\frac{L_{\text{H}\beta}}{10^{42} \text{ ergs s}^{-1}} \right)^{0.56} \left(\frac{\text{FWHM}(\text{H}\beta)}{1000 \text{ km s}^{-1}} \right)^2 M_{\odot} \quad (3)$$

$L_{\text{bol}}/L_{\text{Edd}}$ is estimated by simply assuming the bolometric luminosity of quasar is proportional to the luminosity at rest-frame wavelength 5100 \AA : $L_{\text{bol}} = 9\lambda L_{\lambda}(5100 \text{ \AA})$ (e.g., Kaspi et al. 2000), where

$$L_{5100} = 2.4 \times 10^{43} \left(\frac{L_{\text{H}\alpha}}{10^{42} \text{ erg s}^{-1}} \right)^{0.86} \text{ erg s}^{-1} \quad (4)$$

For each object, both the luminosities of $H\alpha$ and $H\beta$ are corrected for local extinction according to their observed Balmer decrements. The estimated M_{BH} from $H\alpha$ and $H\beta$ are listed in Table 1, and they are highly consistent with each other within a factor of two

for all the three galaxies, which is less than the typical absolute uncertainties of the mass scaling relationships (Vestergaard & Peterson 2006). It is clear that all the three objects show low $M_{\text{BH}} \sim 10^6 M_{\odot}$ and high $L/L_{\text{Edd}} \sim 0.2$, which implies that the three objects have an NLS1-like nucleus in their galaxy centers.

5. Discussion

The spectral analysis given above clearly reveals that the emission lines of the three objects consist of two components with distinct origins. The narrow emission lines are mainly powered by star formation activity, and the broad emission lines by central AGN. In addition, the AGNs show small M_{BH} , large L/L_{Edd} , and strong Fe II emission, which is typical of NLS1 galaxies (e.g., Zhou et al. 2006).

Except for the AGN’s contribution, other mechanisms may be responsible for the broad line emission in the spectra of these objects, including stellar winds and supernova remnants (e.g. Izotov et al. 2007). Both of these mechanisms can produce broad emission lines with $\text{FWHM} \geq 1000 \text{ km s}^{-1}$. However, the luminosity of $\text{H}\alpha$ broad components for our three objects are $\sim 10^{42} \text{ erg s}^{-1}$, far exceeding the typical luminosity of broad $\text{H}\alpha$ of stellar winds from Wolf-Rayet or luminous blue variable stars (10^{36} - $10^{40} \text{ erg s}^{-1}$). Moreover, if the broad component is caused by supernova events, the magnitude obtained from the spectrum is expected to greatly differ from the photometric magnitude, because the brightness of supernova must decay at the time interval between the two observations of about a year. We obtain the SDSS r' band magnitudes from the observed spectra by convolving each spectrum with the r' band transmission curve, and compare them with the corresponding fiber magnitude obtained in the SDSS. The magnitude difference is found to be less than 1 mag within the interval of about a year for these three objects. As a result, we can eliminate the possibility of Type IIp supernova events.

We propose that the three objects are at the transition stage from the starburst-dominated phase to AGN-dominated phase, which is supported by the theoretical evolutionary scenario given by the numerical simulations of mergers of two gas rich galaxies. Hopkins et al. (2005a, 2005b, and references therein) proposed a scenario that the central black hole of AGN is buried by gas or dust in the young AGN phase. In their analysis, when starbursts are triggered by the nuclear inflow and feed black hole growth, the black hole is heavily obscured by surrounding gas or dust. As the black hole grows, the black hole feedback will blow the gas or dust away in a powerful wind, and the luminous AGN will be seen at that time. A case for the model is NGC 6240, of which the X-ray data reveal that there are two AGNs, while the optical data cannot resolved them, possibly for the reason that the

AGNs are in highly dust-enshrouded environments (e.g. Komossa et al. 2003; Gressen et al. 2004; Max et al. 2005). We believe that the next generation hard X-ray missions with enhanced capability (in sensitivity and imaging), such as NuSTAR, Simbol-X and NeXT, would be helpful in identifying and studying the starburst obscured AGNs.

Finally, we need to understand why the emission from AGN NLR is so weak that the narrow emission is overwhelmed by the contribution from H II region. Netzer et al. (2004, and see also in Netzer et al. 2006) proposed that the NLR would be dynamically unbounded if the AGN luminosity is high enough. The distance of the NLR, if it exists, from the central black hole is estimated to be not far less than 1kpc for the three objects according to the relationship $R_{\text{NLR}} = 1.15 L_{\text{H}\beta,42}^{0.49}$ kpc (Netzer et al. 2004), where $L_{\text{H}\beta,42} = L_{\text{H}\beta}/10^{42}$ erg s⁻¹. At this distance, the escape velocity for a spherical galaxy roughly equals to $290 M_{*,11}^{1/2} R_{10\text{kpc}}^{-1/2}$ km s⁻¹, where $M_{*,11}$ is the stellar mass in units of $10^{11} M_{\odot}$, and $R_{10\text{kpc}}$ the radial distance in units of 10kpc. The stellar mass could be inferred from the the estimated mass of the SMBH according to the well-established black hole and bulge mass relation $\langle M_{\text{BH}}/M_{*} \rangle \sim 0.002$ (McLure & Dunlop 2004), which results in an escape velocity only ~ 100 km s⁻¹. This scenario is supported by recent observation study of extended emission-line regions (EELRs) around low-*z* QSOs. Husemann et al. (2008) found that the presence of EELRs are preferentially detected in QSOs with large black hole masses.

The lack of typical NLR in the three objects leads us to suspect that the NLR might evolve with AGN and its host galaxies. Netzer et al. (2004) proposed a scenario of “star-forming NLRs” in which the compact NLR gas in kpc scale is caused by the star formation activity. An alternative possible scenario proposed here is that the the formation of NLR is the consequence of the feedback of central AGNs. As discussed above, a powerful feedback wind is required for AGNs to dispel the surrounding gas and dust material to appear as a luminous AGN at about 1 Gyr since the merger (Hopkins et al. 2005a). This implies the typical NLR would not emerge until a majority of surrounding material has been dispelled. Another implication for the wind scenario is that the NLR kinematics is dominated by radial outflow. In fact, spectroscopic studies with high spatial resolution of NLR of a few nearby Seyfert 2 galaxies indicate that radial velocity fields can be modeled by biconical outflows where the NLR gas accelerates outward from the nucleus to a turnover point at a distance of ~ 100 pc from the nucleus and subsequently appears to decelerate to the systemic velocity at a distance of ~ 300 pc (e.g., Hutchings et al. 1998; Kaiser et al. 2000; Nelson et al. 2000; Crenshaw et al. 2000; Crenshaw & Kraemer 2000; Ruiz et al. 2001).

6. Conclusions

By studying the optical spectra of the three objects: SDSS J091053+333008, SDSS J121837+091324, and SDSS J153002-020415, we find that all of them are located in the HII region in the BPT diagnostic diagram. However, all of their spectra display characteristic features of AGNs. All of them have large Eddington ratio, small black hole mass, and small SFR. We propose that the dust-buried-AGN (Hopkins et al. 2005a, b) can explain the feature.

We would thank the anonymous referee for constructive comments that improved the paper. We are grateful to Todd A. Boroson and Richard F. Green for providing us the FeII template. This work was supported by the National Science Foundation of China (grant 10803008 and 10873017) and National Basic Research Program of China. The SDSS archive data is created and distributed by the Alfred P. Sloan Foundation. This research has made use of the NASA/IPAC Extragalactic Database, which is operated by JPL, Caltech, under contact with the NASA.

REFERENCES

- Adelman-McCarthy, J. K., et al. 2006, *ApJS*, 162, 38
- Balogh, M. L., et al., 1999, *ApJ*, 527, 54
- Boroson, T. A., & Green, R. F., 1992, *ApJS*, 80, 109
- Boroson, T. A., 2002, *ApJ*, 565, 78
- Boroson, T. A., 2005, *ApJ*, 130, 381
- Brotherton, M. S., van Breugel, Wil., Stanford, S. A., et al., 1999, *ApJ*, 520, L87
- Bruzual. G., & Charlot. S., 2003, *MNRAS*, 344, 1000
- Canalizo, G., et al., 2006, *NewAR*, 50, 650
- Cardelli, J. A., Clayton, G. C., & Mathis, J. S., 1989, *ApJ*, 345, 245
- Crenshaw, D. M., et al. 2000, *AJ*, 120, 1731
- Crenshaw, D. M., & Kraemer, S. B. 2000, *ApJ*, 532, L101

- Di Matteo, T., et al., 2005, *nature*, 433, 604
- Ferrarese, L., et al. 2006, *ApJ*, 644, L21
- Gallagher, J. S., Hunter, D. A., & Bushouse, H., 1989, *AJ*, 97, 100
- Goncalves, A. C., Veron-Cetty, M. P., & Veron, P., 1999, *A&AS*, 135, 437
- Gonzalez Delgado, R., 2002, *ASPC*, 258, 101
- Goto, T., 2006, *MNRAS*, 369, 1765
- Greene, J. E., & Ho, L. C., 2005, *ApJ*, 630, 122
- Greene, J. E., & Ho, L. C., 2006, *ApJ*, 641, L21
- Gressen, J., et al., 2004, *AJ*, 127, 75
- Hao, L., Strauss, M. A., Tremonti, C. A., et al. 2005, *AJ*, 129, 1783
- Heckman, T. M., Kauffmann, G., Brinchmann, J., et al., 2004, *ApJ*, 613, 109
- Hopkins, P., Hernquist, L., Martini, P., et al. 2005, *ApJ*, 625, L71
- Hopkins, P., Hernquist, L., Cox, T., et al. 2005, *ApJ*, 630, 705
- Hu, C., et al. 2008, *ApJ*, 687, 78
- Hutchings, J. B., et al. 1998, *ApJ*, 492, L115
- Kaiser, M. E., et al. 2000, *ApJ*, 528, 260
- Kaspi, S., et al. 2000, *ApJ*, 539, L13
- Kaspi, S., et al. 2007, *ApJ*, 659, 997
- Izotov, Y. I., Thuan, T. X., & Guseva, N. G., 2007, *ApJ*, 671, 1297
- Kauffmann, G., Heckman, T. M., Tremonti, C., et al., 2003, *MNRAS*, 2003, 346, 1055
- Kennicutt, R. C., 1998, *ARA&A*, 36, 189
- Kewley, L. J., et al. 2001, *ApJ*, 556, 121
- Kewley, L. J., Geller, M. J., & Jansen, R. A., 2004, *AJ*, 127, 2002
- Kewley, L. J., Groves, B., Kauffmann, G., Heckman, T., 2006, *MNRAS*, 372, 961

- Komossa, S., Burwitz, V., Hasinger, G., et al., 2003. *ApJ*, 582, 15
- Komossa, S., Xu, D., Zhou, H., et al., 2008. *ApJ*, 680, 926
- Kriss, G., 1994, in ASP Conf. Ser. 61, *Astronomical Data Analysis Software and Systems III*, ed. D. R. Crabtree, R. J. Hanisch, & J. Bames (San Francisco: ASP), 437
- Li, C., Wang, T. G., Zhou, H. Y., et al. 2005, *AJ*, 129, 669
- Magorrian, J., Tremaine, S., Richstone, D., et al., 1998, *AJ*, 115, 2285
- Mathur, S. 2000, *MNRAS*, 314, L17
- McGill, K. L., et al. 2008, *ApJ*, 673, 703
- McLure, R. J., & Dunlop, J. S., 2004, *MNRAS*, 352, 1390
- Max, C. E., et al., 2005, *ApJ*, 621, 738
- Nelson, C. H. 2000, *ApJ*, 544, L91
- Netzer, H., et al. 2004, *ApJ*, 614, 558
- Netzer, H., et al. 2006, *A&A*, 453, 525
- Osterbrock, D. E., & Pogge, R. W. 1985, *ApJ*, 297, 166
- Osterbrock, D. E., 1989, *Astrophysics of Gaseous Nebulae and Active Galactic Nuclei*, Mill Valley CA: University Science Books
- Riechers, D. A., Walter, F., Carilli, C. L., Bertoldi, F., Momjian, E., 2008, *ApJ*, 686, L9
- Schlegel, D. J., Finkbeiner, D. P., & Davis, M. 1998, *ApJ*, 500, 525
- Shields, G., Gebhardt, K., Salviander, S., et al., 2003, *ApJ*, 583, 124
- Springel, V., et al. 2005, *nature*, 435, 629
- Tremaine, S., et al. 2002, *ApJ*, 574, 740
- Vestergaard, M., & Peterson, B., 2006, *ApJ*, 641, 689
- Walter, F., Carilli, C., & Bertoldi, F., et al. 2004, 615, L17
- Wang, J., Wei, J. Y., & He, X. T., 2006, *ApJ*, 638, 106
- Wang, J., & Wei, J. Y., 2008, *ApJ*, 679, 86

Weedman, D. W., 1983, ApJ, 266, 479

Wild, V., et al. 2007, MNRAS, 381, 543

Worthey, G., & Ottaviani, D. L., 1997, ApJS, 111, 377

Zhou, H. Y., Wang, T. G., Dong, X. B., Wang, J., Lu, H., 2005, Mem, S. A. It 76, 93

Zhou, H. Y., et al. 2006, ApJS, 166, 128

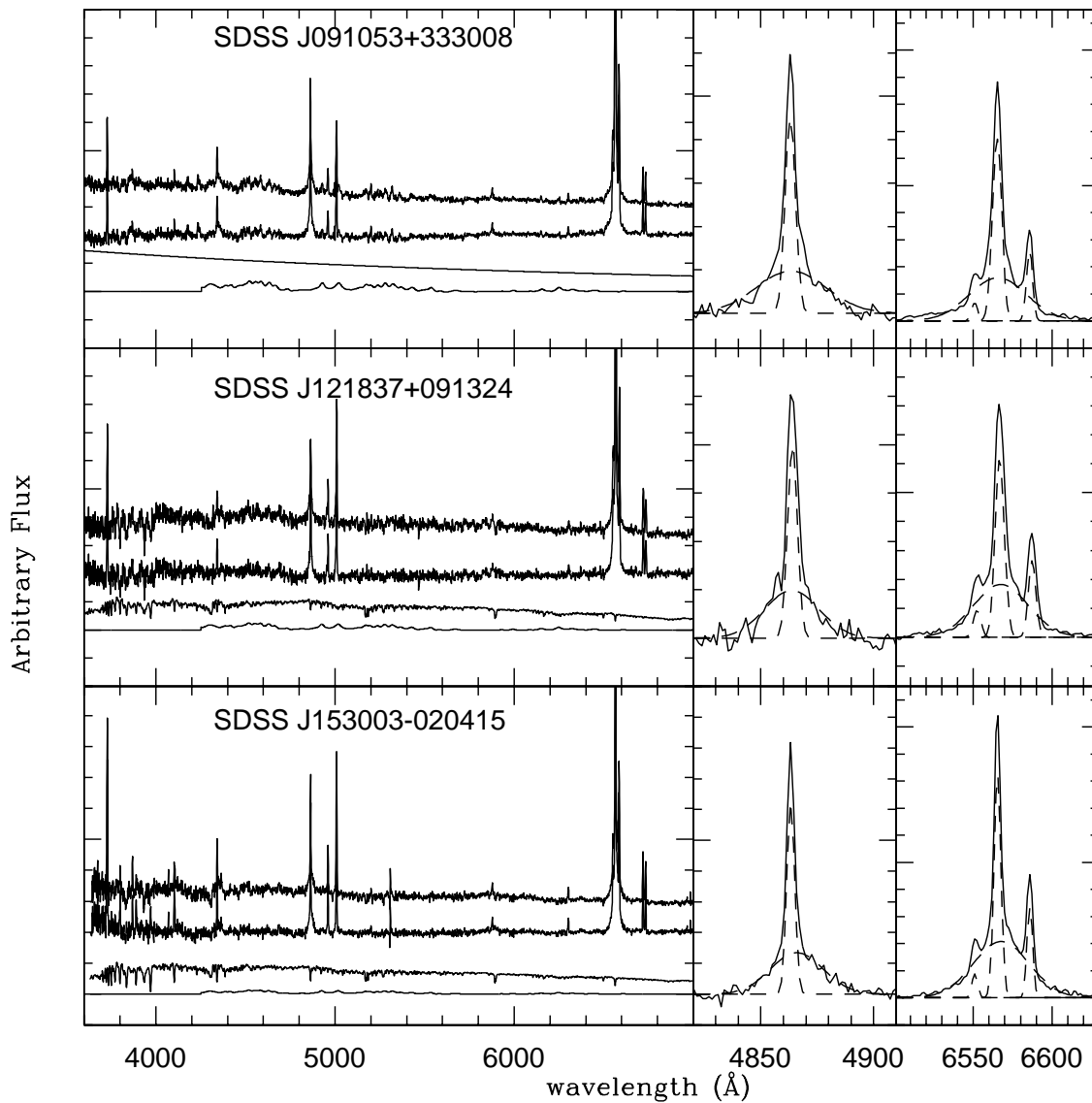


Fig. 1.— left: Detailed modeling and subtractions of the starlight components in the spectra of the three objects. For SDSS J091053+333008, we plot the observed spectrum, emission-line spectrum, a power-law continuum, and FeII blends, from top to bottom. For the other two objects, we plot the emission-line spectrum, observed spectrum, modeled starlight spectrum, and FeII blends. The spectra are vertically shifted by arbitrary amounts for visibility. Middle: Modelings of the two Gaussian profiles for the $H\beta$ region. Right: Modelings of a set of Gaussian profiles for the $H\alpha$ region.

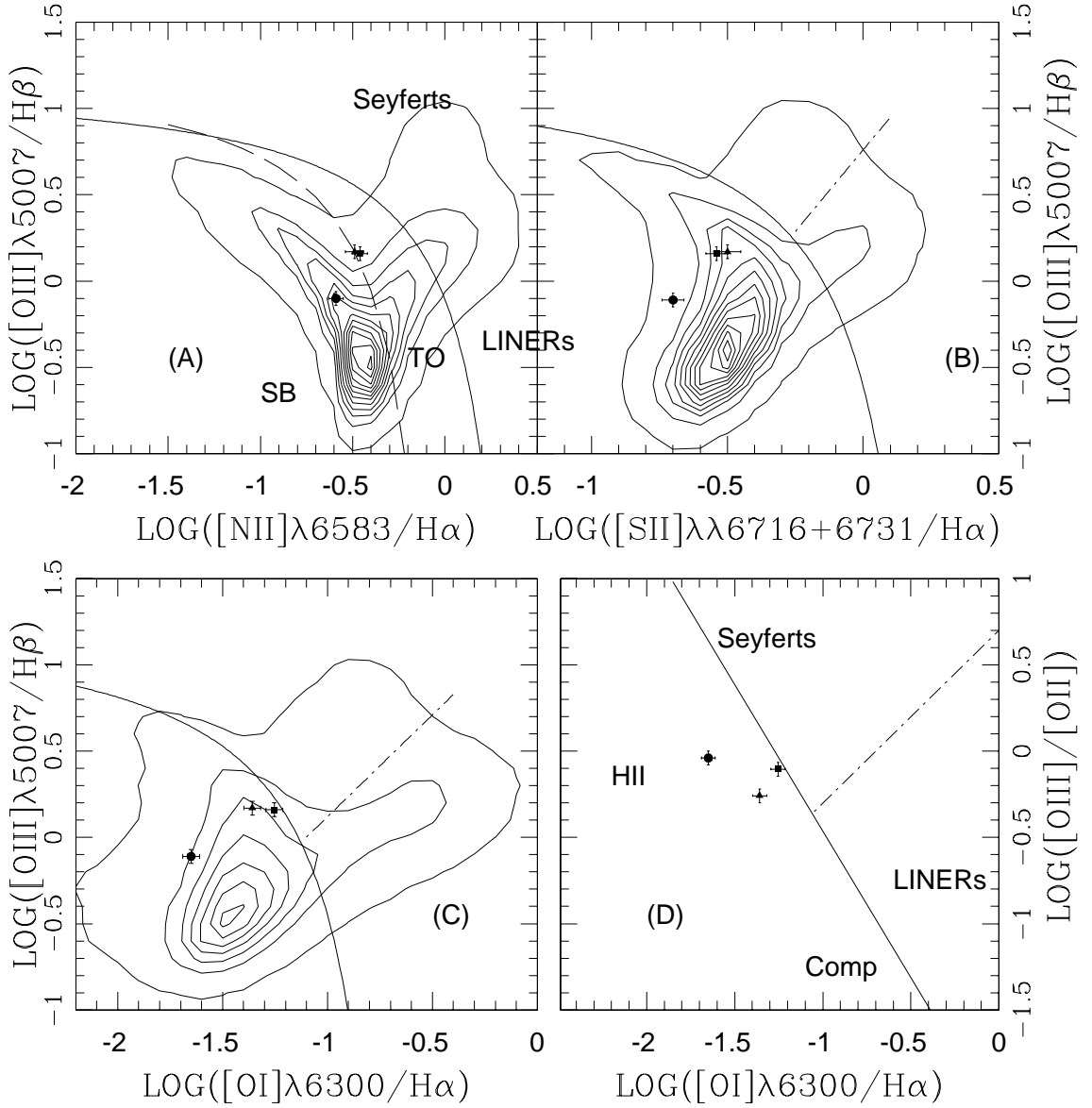


Fig. 2.— The four BPT diagnostic diagrams for our three galaxies. The theoretical lines separating AGNs from star-forming galaxies proposed by Kewley et al. (2001) are shown by the solid lines in all four panels, while the empirical lines proposed by Kauffmann et al. (2003) by the dashed line in Panel A. The dot-dashed lines in Panel B, C, D separating LINERs from Seyferts are proposed by Kewley et al. (2006). The circles are for SDSS J091053+333008, the squares are for SDSS J121837+091324, and the triangles are for SDSS J153002-020415. All of our three galaxies are located in the star-forming region, which is proposed by Kewley et al. (2006).

Table 1: Properties of the emission lines of the three objects, Black hole masses, Eddington Ratios and SFR.

Lines	SDSS J091053+333008	SDSS J121837+091324	SDSS J153002-020415
H β _N	25.8±1.3	11.1±0.7	27.5±2.0
H β _B	37.3±1.7	14.8±0.9	39.5±2.8
[OIII] λ 5007	20.3±0.7	16.1±0.4	41.1±0.5
H α _N	99.5±3.1	45.5±1.5	93.0±4.1
H α _B	148.1±4.0	79.0±2.2	185.8±6.4
[NII] λ 6583	25.3±1.2	15.9±0.7	30.2±2.3
[SII] λ 6716	10.0±0.6	7.8±0.4	17.4±1.4
[SII] λ 6731	9.5±0.6	5.2±0.4	11.8±1.2
[OI] λ 6300	2.2±0.5	2.4±0.5	4.1±0.9
[OII] λ 3727	17.4±1.0	14.8±0.7	65.5±3.5
Rfe	1.7±0.1	2.9±0.2	0.1±0.0
FWHM(H β _B)	2.3±0.2	1.7±0.2	1.7±0.2
A_v	0.70±0.04	0.88±0.04	0.35±0.02
$M_{\text{BH}}(\text{H}\alpha)/10^6 M_{\odot}$	7.9±2.0	3.2±0.7	2.8±0.6
$M_{\text{BH}}(\text{H}\beta)/10^6 M_{\odot}$	9.9±2.4	2.3±0.7	1.7±0.6
$L_{\text{bol}}/L_{\text{Edd}}$	0.21±0.04	0.16±0.03	0.13±0.03
SFR	2.4±0.1	0.8±0.0	0.6±0.0

Notes: The flux of each component is in the unit of $10^{-16} \text{ergs s}^{-1} \text{cm}^{-2}$. The FWHM(H β) is in the unit of 10^3km s^{-1} . And the SFR is in the unit of $M_{\odot} \text{yr}^{-1}$